PAIN®

Activation of the dorsal, but not the ventral, hippocampus relieves neuropathic pain in rodents

Xuhong Wei[a,b], Maria Virginia Centeno[b], Wenjie Ren[b], Anna Maria Borruto[b], Daniele Procissi[c], Ting Xu[a], Rami Jabakhanji[b], Zuchao Mao[b], Haram Kim[b], Yajing Li[d,e,f], Yiyuan Yang[d,e,f], Philipp Gutruf[d,e,f], John A. Rogers[d,e,f], D. James Surmeier[b], Jelena Radulovic[g], Xianguo Liu[a], Marco Martina[b,g], Apkar Vania Apkarian[b,h,i,*]

Abstract

Accumulating evidence suggests hippocampal impairment under the chronic pain phenotype. However, it is unknown whether neuropathic behaviors are related to dysfunction of the hippocampal circuitry. Here, we enhanced hippocampal activity by pharmacological, optogenetic, and chemogenetic techniques to determine hippocampal influence on neuropathic pain behaviors. We found that excitation of the dorsal (DH), but not the ventral (VH) hippocampus induces analgesia in 2 rodent models of neuropathic pain (SNI and SNL) and in rats and mice. Optogenetic and pharmacological manipulations of DH neurons demonstrated that DH-induced analgesia was mediated by N-Methyl-D-aspartate and μ-opioid receptors. In addition to analgesia, optogenetic stimulation of the DH in SNI mice also resulted in enhanced real-time conditioned place preference for the chamber where the DH was activated, a finding consistent with pain relief. Similar manipulations in the VH were ineffective. Using chemo-functional magnetic resonance imaging (fMRI), where awake resting-state fMRI was combined with viral vector-mediated chemogenetic activation (PSAM/PSEM[89s]) of DH neurons, we demonstrated changes of functional connectivity between the DH and thalamus and somatosensory regions that tracked the extent of relief from tactile allodynia. Moreover, we examined hippocampal functional connectivity in humans and observe differential reorganization of its anterior and posterior subdivisions between subacute and chronic back pain. Altogether, these results imply that downregulation of the DH circuitry during chronic neuropathic pain aggravates pain-related behaviors. Conversely, activation of the DH reverses pain-related behaviors through local excitatory and opioidergic mechanisms affecting DH functional connectivity. Thus, this study exhibits a novel causal role for the DH but not the VH in controlling neuropathic pain–related behaviors.

Keywords: Hippocampus, Neuropathic pain, Glutamate, GABA, Opioids, fMRI, Wireless optogenetics, Analgesia

1. Introduction

Besides the well-known roles in memory storage and spatial navigation,[23,46] the hippocampus also plays central roles in emotional processes, stress responses,[26,50] fear context attribution,[41] and autonomic regulation.[47] Accumulating evidence, over the past 2 decades, continues to demonstrate differential organization of the hippocampus along its long axis (septotemporally or dorsoventrally in rodents and posteroanteriorly in primates) regarding extrinsic and intrinsic physiological properties, anatomical inputs and outputs, as well as genetic and functional

differences.[51,54,56,70,76] A prevailing viewpoint is that the dorsal (DH) (or posterior, PH) hippocampus is better implicated in episodic memory and spatial navigation,[25,57,71] and the ventral (VH) (or anterior, AH) hippocampus is a critical component of the anxiety network[1,19,33] (although components of anxiety are also captured within the DH/PH[64,65]). Consistent with this viewpoint is evidence of a differential increase of neurosteroid precursors in the VH (relative to the DH) and the anxiolytic effects of hippocampal neurosteroids in neuropathic pain.[82] Involvement of the DH in acute and chronic pain phenotypes is also supported: nonsteroidal

anti-inflammatory drugs microinjection into the DH induces antinociception[29] and also by microinjection of carbachol, morphine, and bicuculline into the DH, whereas muscimol injections enhance nociception.[27] In keeping with these findings, multiple hippocampal dysfunctions have been identified in rodent models of neuropathic pain, including impaired synaptic plasticity, decreased expression of N-Methyl-D-aspartate (NMDA) receptor subtypes, neurogenesis, instability of place cells, and reorganization of resting-state connectivity.[5,11–13,42,49,62,78] Moreover, adult hippocampal neurogenesis appears a critical mechanism controlling the transition to chronic pain,[3] and hippocampal expression of the proinflammatory cytokine IL-1β increases in neuropathic rats, and its expression level is positively correlated with tactile allodynia (pain-like behavior).[21] These findings are complemented by observations in human pain patients, where low hippocampal volumes seem a feature of multiple chronic pain conditions[74] and the hippocampal volume itself appears to be a predictive factor for transitioning from subacute to chronic back pain.[74] Thus, hippocampal physiology and connectivity undergo large adaptations with the establishment of chronic pain. Yet, how these changes influence on the ability of the hippocampal circuitry to control pain behavior remains unclear, and whether the DH and VH are differentially involved in pain phenotypes remains unexplored.

We hypothesized that hippocampal adaptations with the transition to chronic pain, specifically after a peripheral neuropathic injury, would enhance the involvement of the hippocampal circuitry in pain behaviors. We test this hypothesis by studying the modulation of exaggerated tactile responses in mouse and rat models of neuropathic pain, after local activation of DH or VH neurons, with microinjection of glutamate, by optogenetic excitation using channelrhodopsin-2 (ChR2), or by enhancing depolarizing currents chemogenetically (PSAM/PSEM[89s]). We use wireless optogenetics to assess sensory and affective/motivational aspects of neuropathic pain (optodriven real-time conditioned place preference [opto-rtCPP]); and in rats, we combine chemogenetic manipulations with awake resting-state functional magnetic resonance imaging (fMRI) (chemo-fMRI)[28] to identify the impact of hippocampal connectivity in the modulation of neuropathic pain behaviors.

2. Methods

2.1. Animals

For these experiments, we used Sprague-Dawley rats weighing 200 to 250 g and adult male C57BL/6 mice weighing 25 to 31 g. The animals were group-housed and had free access to standard chow and water. Some of the described experiments were performed in Sun Yat-sen University, Guangzhou, China, whereas others were performed in Northwestern University, Chicago. At both locations, the animals were kept at $21 \pm 2°C$ temperature and 30% to 60% humidity, under a 12/12-hour light/dark cycle. Handling and testing were performed during the light period. To minimize stress, they were handled regularly before surgery and behavioral testing. All studies were approved by the Animal Care and Use Committee of Northwestern University or by the Local Animal Care Committee (Sun Yat-sen University) and followed the ethical guidelines for the investigation of experimental pain in conscious animals.

2.2. Neuropathic pain models

2.2.1. Spared nerve injury

Spared nerve injury (SNI) was performed following the original description.[20] Briefly, rats were anesthetized with isoflurane (1.5%-

2.5%) in a mixture of 30% N_2O and 70% O_2. The sciatic nerve of the left leg was exposed at the trifurcation of peroneal, tibial, and sural branches. The common peroneal and tibial nerves were ligated and cut, whereas the sural nerve was left intact. For the animals in the sham group, the sciatic nerve was only exposed but not disturbed.

2.2.2. Spinal nerve ligation

Lumbar segment 5 spinal nerve ligation (SNL) was performed following the original description.[35] Briefly, after rats were anesthetized with isoflurane (1.5%-2.5%), the L5 transverse process was removed to expose the left L5 spinal nerve. L5 spinal nerve was then isolated carefully and ligated tightly with 6-0 silk thread, 5 to 10 mm distal to the L5 dorsal root ganglion.

2.3. Drug administration through brain microinjection

L-Glutamate acid and monosodium salt monohydrate, D(−)-2-amino-5-phosphonopentanoic acid (AP5), were purchased from Sigma (St. Louis, MO). Indiplon was purchased from Cayman Chemical (Ann Arbor, MI). For the brain microinjections, rats were anesthetized with sodium pentobarbital (50 mg/kg, intraperitoneally [i.p.]), and permanent guide cannulae (23 gauge) were implanted in the DH or VH, ipsilateral to the peripheral injury. The stereotaxic coordinates were: AP −3.5 mm, ML −2.0 mm, and DV −3.2 mm (DH); and AP −4.8 mm, ML 4.6 mm, and DV −8.1 mm (VH).[52] Cannulae were secured with dental cement and anchored to stainless-steel screws fixed to the skull. To prevent clogging and infection, a stainless-steel obturator was inserted into the guide cannula. The rats were allowed to recover for 6 days after surgery. Drug infusions (in a volume of 1 μL) were performed into the DH or VH, ipsilateral to the peripheral injury using a Hamilton syringe connected to a 30-gauge injector at a speed of 1 μL over 1 minute, while the rats were lightly restrained. The injection needle was kept in place for 1 minute to allow the drug to completely diffuse from the tip, and then, the obturator was reinserted into the guide cannula. AP5 (in a volume of 1 μL) was injected through the cannula placed in the DH 30 minutes before glutamate injection. All injection sites were verified post hoc.

2.4. Assessment of mechanical allodynia

Mechanical response thresholds of the animals were assessed before and after neuropathic injury with the up-down method.[18] Briefly, animals were placed in a Plexiglass box with a wire grid floor and allowed to habituate to the environment (10-15 minutes for rats and 40-55 minutes for mice). Von Frey (VF) filaments of varying forces (Stoelting Co Wood Dale, IL. USA) were applied to the lateral plantar surface of the hind paw. Filaments were applied in either ascending or descending strengths to determine the filament strength closest to the hind paw withdrawal threshold. Each filament was applied for a maximum of 2 seconds at each trial; paw withdrawal during the stimulation was considered a positive response. Given the response pattern and the force of the final filament, 50% paw withdrawal threshold was calculated following the method described by Chaplan et al.[18]

2.5. In vivo optical stimulation of the DH or VH

Adult male C57BL/6 mice (6-8 weeks old) were used for these experiments. Stereotaxic-guided (Kopf Instruments, Tujunga, CA) virus injections were performed as described above. Mice were injected unilaterally (ipsilateral to the peripheral injury) with 250 nL of AAV5-Syn-ChR2-eYFP (Hope Center Viral Vector Core, viral titer 2

$\times$ 10^{13} vg/mL) into the DH (bregma -1.85 mm; lateral -1.0 mm; ventral -2.0 mm) or VH (bregma -3.5 mm; lateral -2.9 mm; ventral -4.35 mm). The injection pipette was withdrawn 5 minutes after the infusion, and the scalp was then sealed. After allowing 3 weeks for sufficient ChR2 expression, mice skulls were implanted in the injected area with thin, flexible, light weight, battery-free, wirelessly powered μ-ILED (Cree, Inc Durham, NC, USA, 470 nm in wavelength, 220 $\times$ 270 $\times$ 50 μm) devices. Each device contains a power receiving coil with diameter $\sim$10 mm. The needle portion of the device incorporating the μ-ILED interconnects with the coil through stretchable serpentine traces and can be inserted into the DH or VH, as previously described.[68] Briefly, the coordinates of the needle tips of the devices are 200 μm lateral and deeper than the coordinates for the virus injections. The device was fixed in place using a small amount of cyanoacrylate gel. All mice were single housed for 3 days after the implantation and were then put back with their former littermates. The devices remained intact and provide a robust optical performance while implanted in the targeted areas.

Spared nerve injury surgeries were performed 1 week after hippocampal fiber implantation. Prestimulation baselines for paw withdrawal threshold and place preference were assessed on post-SNI day 7. The wireless photostimulation-paired rtCPP tests were performed on post-SNI day 8 to 11 (twice per day). Paw withdrawal thresholds were examined on post-SNI day 30. The DH and VH were stimulated using wireless photostimulation devices (Neurolux, Urbana, IL; output 7 W, 2-ms pulses at a 20 Hz frequency). Channelrhodopsin-2 expression was verified post hoc using fluorescence microscopy on brain sections.

2.6. Real-time conditioned place preference test using optical stimulation

The CPP apparatus consists of 2 connected compartments (30 $\times$ 30 $\times$ 30 cm each) with distinct tactile and visual cues. On the prestimulation session (Pre-stim on SNI day 7), the mice were placed into each of the chambers and allowed to freely explore both for 15 minutes, with no stimulation at any time. In subsequent stimulation sessions (Stim S1-S8 from SNI day 8-day 11, twice 15-minute sessions per day), the mouse entry into 1 compartment activated a wirelessly powered photostimulation (Neurolux) operating at 13.56 MHz (wireless system output 7 W, 2-ms pulses, frequency: 20 Hz) as long as the mouse remained in the stimulation-paired compartment, whereas entry into the other compartment did not cause any photostimulation. For each mouse, the less preferred compartment during the preconditioning phase was used as the stimulation-paired assigned side. White noise was played during all sessions to block out any possible extraneous acoustic cues. The time spent in the stimulation-paired side and the time in the center area of the stimulation side were measured in each session using Any-maze tracking software. Preference was calculated as the time in the stimulation-paired side at each stimulation session minus the time in the stimulation-paired side during the prestimulation session.

2.7. Von Frey assessment during continuous optical stimulation

The arena consists of a single compartment (30 $\times$ 30 $\times$ 30 cm). Mice were placed into the chamber and allowed to freely explore it for 15 minutes. During this time, they were continuously stimulated using a wirelessly powered photostimulation (Neurolux). White noise was played during all sessions to block out any possible extraneous acoustic cues. Tactile thresholds were assessed before and after the photostimulation.

2.8. In vivo chemogenetic activation of the hippocampus

Adult (8-10 weeks; 200-250 g) male Sprague-Dawley rats were group-housed until surgery. As previously described,[60] stereotaxic-guided virus injection surgeries were performed under isoflurane anesthesia (1.5%-2.5%) and a mixture of 30% N_2O and 70% O_2 using a stereotaxic instrument (Kopf Instruments). Four small holes (2 per side) were drilled through the skull, and bilateral virus injections were made using a glass injection pipette (Drummond Scientific Company). To activate the DH, we injected AAV9-SYN-PSAM-L141F-Y115F-5HT3HC-GFP (PSAM, titer: 2.19 $\times$ 10^{13} genomes/mL, Virovek IncHayward, CA, USA) bilaterally using the following coordinates (bregma -3 mm; lateral ±1.7 mm; ventral -3.3 mm for the more rostral location; bregma -4.2 mm; lateral ±2.7; ventral -3.3 mm for the more caudal location; 500 nL/side) at a speed of 100 nL per minute. Head posts were implanted 2 to 3 weeks after virus injection. After a 2-week acclimation period, SNI surgeries were performed, and 4 to 5 days after SNI surgery, paw withdrawal thresholds were assessed before and 0.5 to 2 hours after i.p. injection of either saline or PSEM^{89s} (30 mg/kg). After completion of the experiments, the injection sites were verified by immunohistochemistry.

2.9. In vivo chemogenetic activation of the hippocampus combined with naloxone treatment

Adult (8-10 weeks; 200-250 g) male Sprague-Dawley rats were group-housed until surgery. Stereotaxic-guided virus injection surgeries were performed as described above. To activate the DH, AAV9-SYN-PSAM-L141F-Y115F-5HT3HC-GFP (PSAM, titer: 2.19 $\times$ 10^{13} genomes/mL, Virovek, Inc) was injected bilaterally in the anterior and the posterior DH, 500 nL/side. Spared nerve injury/sham surgery was performed 4 weeks after virus injection. Five days after surgery, the rats received an i.p. injection of PSEM^{89s} (30 mg/kg) followed by a second i.p. injection of either naloxone (5 mg/kg) or saline 30 minutes after the first injection. Two days later, rats that had received PSEM^{89s} and naloxone were injected with PSEM^{89s} and saline, and vice versa. The paw withdrawal threshold was assessed before neuropathic injury and then again before and 1 hour after i.p. PSEM^{89s} injection.

2.10. Electrophysiology

Sagittal brain slices containing the hippocampus were obtained from PSAM virus–injected rats. Rats were anesthetized with ketamine/xylazine and perfused transcardially with ice-cold artificial cerebrospinal fluid (CSF; in mM: 125 NaCl, 2.5 KCl, 1.25 NaH$_2$PO$_4$, 2.0 CaCl$_2$, 1.0 MgCl$_2$, 25 NaHCO$_3$, and 25 glucose, saturated with 95% O_2 and 5% CO_2). Brains were rapidly removed and sliced (VT1200S vibratome; Leica Microsystems Chicago, IL, USA), and the slices were then incubated and transferred into the recording chamber. GFP-positive pyramidal neurons were patched and recorded in current clamp. Pipettes (3-5 MΩ in working solution) were filled with (in mM): 140 KMeSO$_4$, 10 KCl, 10 HEPES, 2 Mg$_2$ATP, 0.4 NaGTP, and 10 sodium phosphocreatine. Signals were filtered at 5 kHz and acquired using a 10-kHz sample frequency. PSEM^{89s} was applied to the bath using a gravity-driven application system. Picrotoxin (100 μM), CNQX (10 μM), and D-AP5 (50 μM) were used to block fast synaptic transmission.

2.11. Awake resting-state functional MRI

These experiments closely followed methods we recently described.[15,17]

2.11.1. Head-post implantation

Surgery for head-post implantation was performed under anesthesia. Rats were initially anesthetized with 3.5% isoflurane mixed with 30% N_2 and 70% O_2, and then transferred to a stereotaxic device and mounted using blunt ear bars that do not break the eardrums. Anesthesia was continued at a lower isoflurane concentration (1.5%-2.5%) sufficient to block motor responses to pinching the hind limbs. The head fur was shaved, and the eyes covered with ointment to prevent drying out and corneal infection. After disinfecting the skin overlying the skull, the scalp was cut longitudinally, and the skin retracted from the cranium. The head post was placed at the midpoint of the bregma and lambda and fixed to the skull with dental cement. The skin wound was treated with triple antibiotic ointment. The rats were then released from the stereotaxic frame and kept warm using a heat lamp. After head-post implantation, rats were given at least 2 weeks of rest to recover from the surgical preparation before the start of acclimation procedures.

2.11.2. Acclimation procedure

For awake scanning, rats first received a surgical implantation of a head post to aid stabilization during scanning. They then received acclimation training in which they were first introduced to snuggle sacks until they began to voluntarily walk into them. Subsequently, snuggle sacks were adjusted around the rats for a snug fit. Once acclimated to their snuggle sacks, the rats were transferred to cradles and then secured to cradles with Velcro straps. The head plate was affixed to the head and subsequently secured to sidewalls mounted on the cradle. Rodents were then acclimated to the head restraint with a graded training procedure. Once the rats became used to the device, their head was screwed to the head-plate that was securely mounted on the cradle. To reduce the stress induced by the MRI experimental environment, rodents were exposed to digital recordings of the sounds generated by gradient switching in the magnet during fMRI, so they were familiar with loud and sudden noise that mimics a typical MRI session. Rats were habituated to the body restrain system and the MRI environment in 30-minute sessions/day for 8 to 10 days, within a 2-week period. They were first habituated to the mock scanner box that simulated the MRI scanner environment and, during later times, to the MRI scanner. Rodents were rewarded with treats at the end of each session. The acclimation training was performed after the head-post implantation and before the SNI surgery, and it was repeated after surgery prior the collection of the imaging data.

2.11.3. Awake functional magnetic resonance imaging

On day 4 or 5 after peripheral surgery, each rat underwent a sequence of 3 imaging scans assessed on the same day at baseline (no injection) and the other 2 scans at 1 hour after the systemic injections. The order of the saline and PSEM[89s] injections was randomized between rats, and at least 2-hour period was left between injections to exclude any remaining effect of the drug. A total of 9 rats were used for these experiments. Rats whose head post became detached during retraining sessions were not imaged. In addition, data from 1 rat at baseline session with excessive motion artifacts were likewise discarded. Thus, we retained scans for 7 SNI rats after 1 hour of PSEM[89s] and saline and 6 rats at baseline.

2.11.4. Equipment for awake rodent functional magnetic resonance imaging

The instruments—including MRI holder, cradle, head plate, head post, and mock scanner box—were designed using

SolidWorks software and were three-dimensional printed (ProofX, IL) using a semitransparent, medical grade material (PolyJet photopolymer MED610, Stratasys) that we had previously tested for magnetic susceptibility. Screws (Small Parts) and fastener were made with Ultem PEI polyetherimide. Custom-made "snuggle sacks" were designed to tailor for rats weighing 300 to 400 g. Snuggle sacks included openings that provided access to the head post. More details can be found in Ref. 17.

2.11.5. Magnetic resonance imaging acquisition

All magnetic resonance experiments were performed on a Bruker 7T ClinScan horizontal magnet. A 2-channel volume resonator was used for radiofrequency transmission, and a 2-cm-diameter surface coil was used for signal detection. Blood oxygenation level–dependent (BOLD) contrast-sensitive T2*-weighted echo-planar imaging was acquired for functional images with the following parameters: gradient-echo, 26 oblique transverse slices, repetition time 2007.5 ms, echo time (TE) 18 milliseconds, in-plane resolution 0.348 mm, slice thickness 0.5 mm, and number of repetition 240. Additional images were collected to optimize registration, including a T2-weighted anatomical image, having identical spatial dimension as in the functional images. EKG and body temperature were continuously monitored during all fMRI experiments.

2.11.6. Image preprocessing

Functional MRI data were preprocessed using FSL 5.1 FEAT (FMRIB's Software Library, http://www.fmrib.ox.ac.uk/fsl) default settings and included motion correction with MCFLIRT, interleaved slice timing correction, skull removal, and spatial smoothing (using FWHM) with a Gaussian kernel of 0.7 mm (not default), chosen because it is roughly 1.5 times the largest dimension of the voxel. BOLD time courses were forward and backward band-pass filtered at 0.01 to 0.08 Hz with a fourth-order Butterworth. Functional images were then registered using FLIRT, first to the individual anatomical T2 image with 6 degrees of freedom (not default), and then, this was registered linearly to the standard brain using 12 degrees of freedom. We used an in-house manually drawn template to identify CSF and white matter voxels in a standard brain image. Average time courses from all the white matter and CSF as well as those pertaining to global whole brain signal were extracted using the FSL fslmeans function. Cerebrospinal fluid, white matter, global signals, and 6 motion parameters (3 translation and 3 rotation) were regressed out from the images using FSL's fsl regfilt linear regression function.

2.11.7. Functional networks

We also constructed a functional connectivity (FC) network for the whole brain to examine its properties between PSEM[89s] and saline conditions, especially for the nodes where PSAM was expressed. The procedure closely followed our earlier methodology.[5] Briefly, the brains were segmented to 96 regions of interest (ROIs, 48 per hemisphere) using a standard rat atlas.[67] The time courses of the BOLD signals for all voxels in each ROI were averaged. Resultant average BOLD signals were used to calculate Pearson correlation coefficients between pairs of ROIs resulting in a 96 × 96 correlation matrix per scan. Data from scans 1 and 2, for PSEM[89s] and saline injections (14 scans per condition), were used to determine FC changes between

PSEM^{89s} and saline conditions. We next calculated average correlation matrices of each condition and the absolute difference between the PSEM^{89s} and saline averages. To evaluate the statistical significance of these changes, we used a permutation test, where we randomized the labels of the correlation matrices, and calculated the difference between the new groups. We repeated the randomization 50,000 times to obtain the null hypothesis distribution for each pairwise connection—the distribution of probable changes in the strength of a connection when the groups are not necessarily different. We then used the null hypothesis distributions to select the connections with a statistically significant change (one-tailed P value < 0.05).

2.11.8. Seed-based connectivity

Functional connectivity maps for the 4 seeds where the PSAM virus was injected were generated in Matlab. We extracted the average BOLD time series from 3-voxel radius spheres surrounding the virus injection coordinates from functional images registered to standard space and each average was correlated against all voxels in the brain using Pearson's correlation. Average FC maps across all 4 seeds were then contrasted between PSEM^{89s} and saline injection conditions (paired within rat contrasts). We then performed a higher-level analysis to identify FC changes correlated with the changes in allodynic threshold of the injured paw between PSEM^{89s} and saline conditions. Individual rat FC difference maps (PSEM^{89s} vs saline) were correlated with change in tactile allodynia between PSEM^{89s} and saline. FSL FLAMEO was again used to identify z-stat maps, corrected for multiple comparisons using intensity $z > 2.3$ and cluster $P < 0.05$ thresholds. The analysis just described constituted the discovery phase, which was based on 1 set of fMRI scans collected in each rat, at 1 hour after PSEM^{89s} or saline injections. We also collected a second fMRI scan immediately after termination of the first, and this scan was reserved for a replication analysis. Preprocessing and postprocessing steps for the replication data were identical to those used for the discovery phase. However, resultant maps were not thresholded, as we only extracted FC values for the regions of interest. These replication maps, reflecting individual rat-, seed-, and condition-specific outcomes, were used to extract FC values at the coordinates of interest derived from the discovery results. Resultant regions were considered to be reproducibly, and with minimal bias, reflecting tactile changes only if the joint P value, for observed correlations between discovery and replication, was significant at $P < 0.0025$ (0.05*0.05). Only 3 (of 8 tested; 4 positive and 4 negative FC changes) regions survived this criterion.

In the virus-injected rats, we collected one more resting-state fMRI immediately after determining tactile thresholds 4 to 5 days after SNI, but just before saline or PSEM^{89s} injections. We used the same preprocessing and postprocessing steps for these scans as well. These data were only used to extract the mean FC map across the 4 seeds.

2.12. Data quantification and statistics

Data were expressed as mean ± SEM (for before–after comparisons) or as median and quartiles (for a small number of observations). One-way or two-way analysis of variance with repeated measures followed by post hoc tests for mean ± SEM data and the paired t test for before–after data was performed to analyze the behavioral outcomes. The criterion of statistical significance was $P < 0.05$. Although no power analysis was performed, the sample size was determined according to peers' and our previous publications in behavioral and pertinent molecular studies. No randomization was used for data collection, but all initial analyses were performed blinded to the condition of the experiments. All brain imaging maps were corrected for multiple comparisons, and the final regions of interest were limited to ones that survived our rigorous discovery and replication procedure.

3. Results

3.1 Pharmacologic manipulation of hippocampal excitability

To establish the role of the hippocampus in the neuropathic pain phenotype, we first tested the effect of local injection of the excitatory neurotransmitter glutamate (21.2 pmol in 1 μL volume) into either the DH or the VH (ipsilaterally to the peripheral SNI) on tactile allodynia in male sham-operated and SNI-operated rats. We found that glutamate injection into the DH had a potent analgesic effect in SNI where the decrease in the tactile threshold was almost completely reversed (tactile threshold increased by >9 folds; $P < 0.001$), but the same injection had minimal effects in sham rats (tactile threshold increased only by ~20%; $P = 0.09$, **Fig. 1A**). Interestingly, the effect of a single injection in SNI rats lasted for up to 2 days, after which it was fully reversed to initial allodynia levels. This pattern was fully reproduced with a second injection, a few days after recovery from the first injection, where we observed complete relief of tactile allodynia for 2 days (**Fig. 1A**). Reversal of tactile allodynia with glutamate injection in the DH (ipsilateral to SNI) was replicated in female rats and also when glutamate was injected in the DH contralaterally or bilaterally relative to the SNI side (Fig. S1, available at http://links.lww.com/PAIN/B350). We also found that the effect of glutamate injection into the DH was dose dependent, reducing the dose resulted in pain relief lasting only for 1 day (5.3 pmol in 1 μL), and this analgesia was abolished if the NMDA antagonist AP5 was injected 30 minutes before glutamate (**Fig. 1B**), thus showing that the glutamate effect requires the activation of NMDA receptors. Next, we investigated whether pharmacological inhibition of the hippocampus would modulate tactile allodynia in SNI. To this end, 2 new cohorts of rats were microinfused with indiplon (5.3 pmol in 1 μL), a positive allosteric modulator of GABA$_A$ receptors,[53] using the same DH and VH coordinates as used for the glutamate injections. In contrast with the glutamate effect, indiplon injection into the DH had no effects in SNI rats but caused a transient proalgesic effect in sham rats (**Fig. 1C**). Importantly, the glutamate effect was reproducible also in SNL rats (**Fig. 1E**), a different model of neuropathic pain.[6] Next, we used the same pharmacological approach to test whether the modulation of the VH similarly affects pain perception in SNI and sham rats. In contrast with the DH data, neither glutamate (**Fig. 2A**) nor indiplon (**Fig. 2C**) injections into the VH produced any detectable effect on tactile allodynia. Taken together, the data show a clear dichotomy between the DH and VH with regard to the modulation of neuropathy-induced tactile allodynia. However, intrahippocampal drug injections have known pitfalls that complicate the interpretation of the functional outcomes. One drawback is that the speed and extent of the drug spread are hard to predict and to measure. Consequently, the effective drug concentration is unclear, which is an important concern particularly when dealing with desensitizing receptors. In addition, the precise time constant of the effect onset and offset relative to neuronal activity may be difficult to determine.

3.2. Optogenetic manipulation of hippocampal activity

To overcome, at least in part, uncertainties associated with pharmacology, we designed a set of experiments to selectively modulate hippocampal excitability using an optogenetic approach.
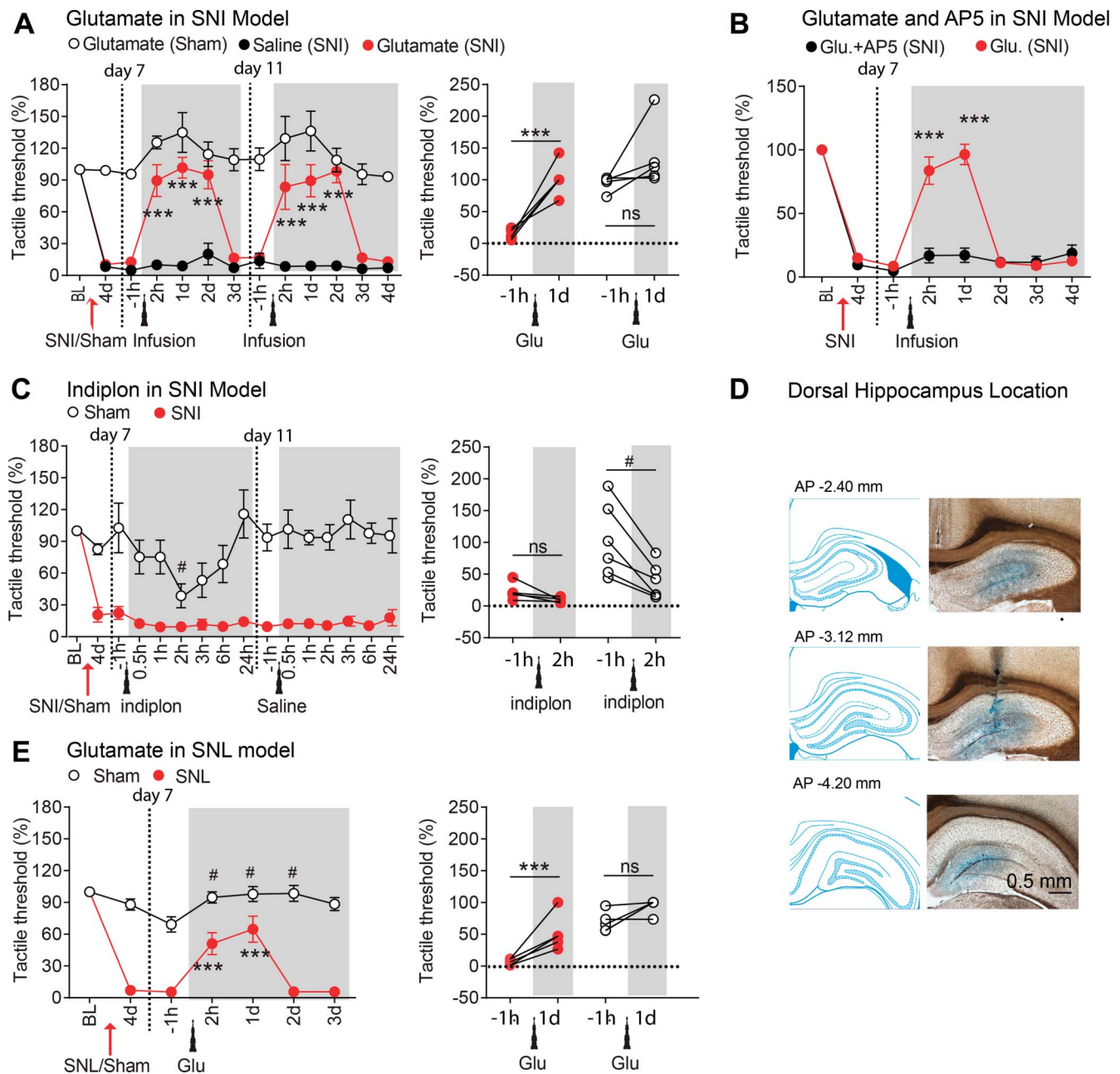
Figure 1. Glutamate, but not indiplon, in the dorsal hippocampus reversed pain-like behaviors after SNI or SNL neuropathic injuries in rats. (A) Microinjection of glutamate (21.2 pmol in 1 μL volume) but not saline into the dorsal hippocampus (ipsilateral to SNI) reversed SNI-induced tactile allodynia. This effect lasted for 2 days and was replicated by a second injection of glutamate (n = 6 rats per group). (B) Coapplication of glutamate (5.3 pmol) with NMDA receptor antagonist APV in the dorsal hippocampus (5 nmol in 1 μL volume, 30 minutes before 5.3 pmol glutamate injection) diminished the effect of glutamate on SNI-induced tactile allodynia (n = 9 rats per group). Note the lower dose of glutamate resulted in shorter duration pain relief. (C) In Sham but not in SNI rats, activation of GABA$_A$ receptors in the dorsal hippocampus by infusion of indiplon (positive allosteric modulator of GABA$_A$ receptors, 10 pmol in 1 μL volume) decreased the tactile thresholds (n = 6 rats per group). (D) Representative coronal sections and histological verification for implanted cannulas. (E) In L5 SNL-induced neuropathic pain model, tactile allodynia on ipsilateral hind paws was reversed by glutamate microinjected into the dorsal hippocampus (5.3 pmol in 1 μL volume, n = 6 per group). Post hoc statistical significance of differences is indicated as follows: ***$P < 0.0001$ and ns $P > 0.05$ (compared with −1 hour before glutamate injection), #$P < 0.05$ (compared with the glutamate-treated SNI group at corresponding time from the start of testing). For detailed statistics, see Table S1, available at http://links.lww.com/PAIN/B350. SNI, spared nerve injury; SNL, spinal nerve ligation.

To this end, AAV-ChR2-GFP was injected into either the DH or the VH of sham and SNI mice (**Fig. 3A**). Acute slice recordings confirmed that ChR2 was expressed and functional in hippocampal neurons (**Fig. 3B**). Similar to the pharmacological manipulations, tactile allodynia was inhibited by optogenetic stimulation of the DH, but not the VH (**Figs. 3C and D**). Thus, both pharmacological and optogenetic activation of the DH (but not the VH) reversed tactile allodynia in SNI rodents. Note the pharmacologic manipulation of the

DH and VH was tested at 7 and/or 11 days after SNI/sham surgeries, whereas continuous DH or VH optogenetic activation was tested at 28 and 23 days after SNI, respectively. Although the time from peripheral injury to optogenetic activation does not match between DH and VH experiments, the DH study resulted in analgesia was at a later time (day 28); thus, the negative results seen with VH stimulation (day 23) cannot be due to virus inefficiency. More importantly, DH-dependent pain relief at 28 days after SNI suggests that the DH
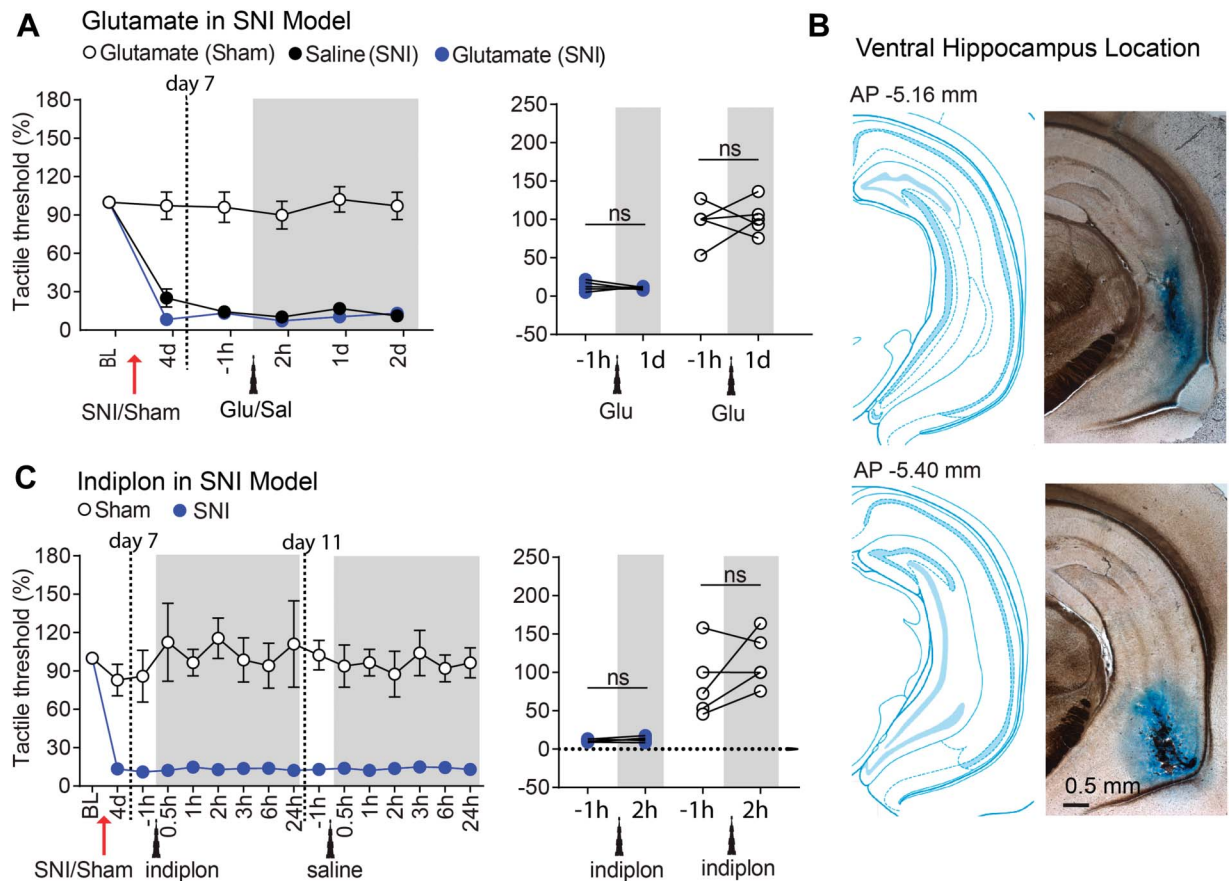
Figure 2. Pharmacological modulation by glutamate or indiplon in the ventral hippocampus had no effect on the tactile thresholds in either SNI or Sham rats. (A) Ventral hippocampus microinjection of glutamate (21.2 pmol in 1 μL volume) or saline did not change the tactile thresholds in either Sham or SNI rats (n = 5 per group). (B) Representative coronal sections and histological verification for implanted cannulas. (C) Indiplon (10 pmol in 1 μL volume) in the ventral hippocampus had no effect on the tactile thresholds in either Sham or SNI rats (n = 5 per group). ns $P > 0.05$ (compared with −1 hour before glutamate or indiplon injections). For detailed statistics, see Table S1 for all statistical tests, available at http://links.lww.com/PAIN/B350. SNI, spared nerve injury.

control of neuropathic pain is persistent for a duration where the condition may be considered transitioning to a more chronic state.[16]

Tactile allodynia, however, only represents one of many symptoms of neuropathic pain. To investigate whether other behaviors are similarly modulated, we took advantage of *wireless real-time place preference* (opto-rtCPP) experiments to test whether optogenetic stimulation of the hippocampus affects place preference in SNI mice. It should be noted that opto-rtCPP has the added advantage that both the hippocampus stimulation paradigm and behavior assessment are fully automated; thus, obtained results should be minimally contaminated with operator influences. In keeping with the findings on tactile allodynia, optogenetic activation of the DH, but not the VH, induced strong preference for the stimulated chamber in SNI, but not sham, mice (**Fig. 4**). Therefore, opto-rtCPP uncovers motivated behavior exhibiting preference for DH (not VH) stimulation only in SNI (not sham) mice. Thus, all the data concur that activation of the DH, but not the VH, improves pain-related phenotypes in neuropathic animal models, without apparent effects in sham-operated animals.

3.3. Chemogenetics and functional magnetic resonance imaging

To prove DH neuronal engagement in neuropathic pain and investigate the identity of the neuronal network underlying the effects induced by hippocampal modulation, we combined chemogenetic tools with awake resting-state fMRI in rats. The

chemogenetic approach, in contrast to pharmacological or optogenetic methods, is a more subtle and specific assessment of the role of infected neurons in a given condition, as it tests whether unmasking of positive modulation of endogenous excitability of neurons infected by PSAM (by PSEM[89s]) would modify a given behavior and also identify related functional circuitry (chemo-fMRI). Thus, the approach establishes that the infected neurons are engaged in the task and that the level of their excitability (rather than direct activation) is linked to the behavior. To this end, we infected the DH bilaterally at 4 sites, hoping to improve the probability of observing behavioral and fMRI outcomes during increased excitability. First, we verified the efficiency of the viral-mediated expression of excitatory (5-HT3 channel-coupled) PSAM in the DH (**Fig. 5A**) by testing the effect of the PSAM agonist PSEM[89s] (10 μM) on intrinsic excitability of infected hippocampal neurons (**Figs. 5B and C**). Next, we activated the DH by injecting PSEM[89s] (30 mg/kg; i.p.). We found a robust analgesic effect (an increase in the allodynic threshold of the injured paw) in SNI rats, which was never detected in PSAM-infected rats that received saline injections or in PSEM-injected sham-operated rats (**Fig. 5D**). Thus, chemogenetic, optogenetic, and pharmacological activation of the DH all have similar effects. Finally, we tested whether the DH effect on tactile allodynia could be linked to the activation of opioid receptors. To this end, we treated PSAM-expressing SNI and sham rats
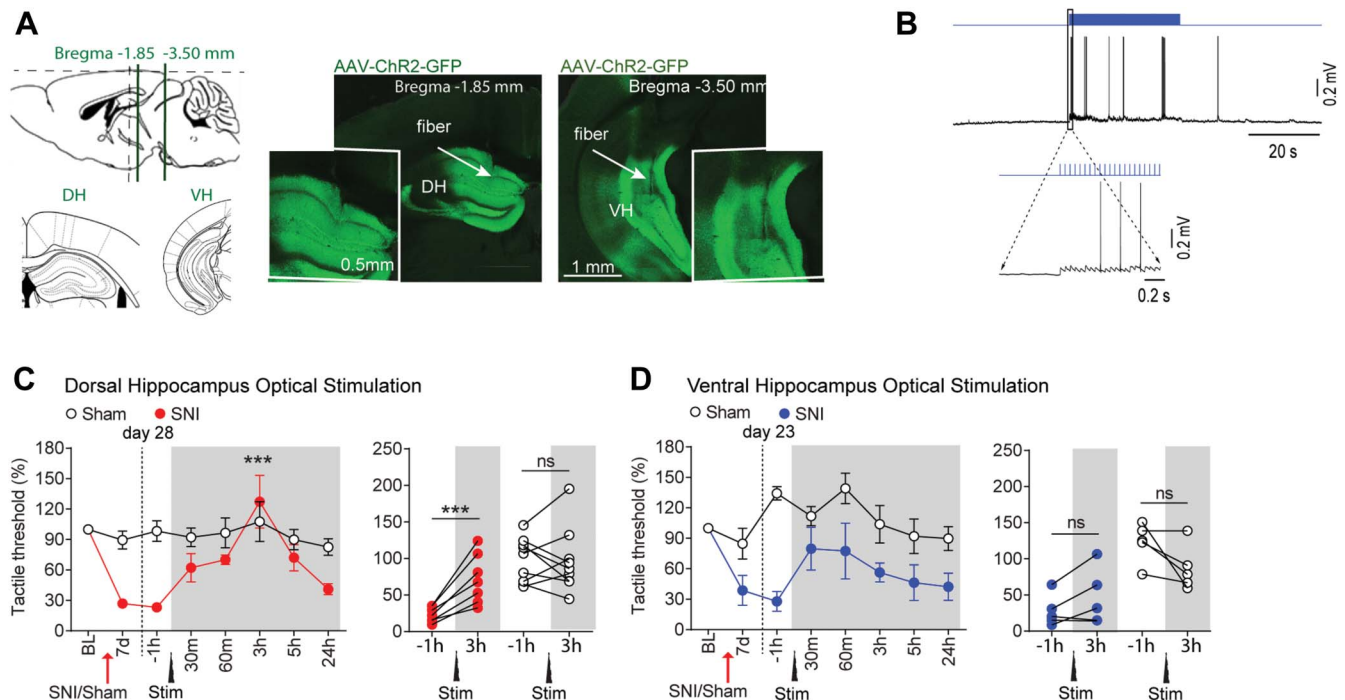
Figure 3. Continuous optogenetic activation of the dorsal, but not the ventral, hippocampus alleviated tactile allodynia in SNI mice. (A) Sample slices display expression of ChR2-GFP in virus injection sites: dorsal hippocampus (DH, left) or ventral hippocampus (VH, right). Intended targets, relative to the bregma, for implanting the optical device are shown in smaller images. (B) Slice recording shows depolarization and spiking evoked in GFP-positive dorsal hippocampal neurons with photostimulation. (C) On SNI day 28, continuous photostimulation of dorsal hippocampal neurons is sufficient to relieve tactile allodynia, at around 3 hours after dorsal hippocampus stimulation (20 Hz stimulation for 15 minutes, n = 7). No effect is observed in Sham mice (n = 9). (D) On SNI day 23, a similar but smaller effect was detected with ventral hippocampus stimulation (20 Hz stimulation for 15 minutes). Hippocampal stimulation is ineffective on Sham mice (n = 5 mice per group). Post hoc statistically significant differences are indicated as follows: *** $P < 0.0001$ and ns $P > 0.05$ (compared with −1 hour before stimulation). For detailed statistics, see Table S1, available at http://links.lww.com/PAIN/B350. SNI, spared nerve injury.

with either saline or the μ-opioid receptor antagonist naloxone (5 mg/kg; 30 minutes after a 30 mg/kg PSEM[89s] i.p. injection; **Fig. 5E**). After another 30 minutes, we tested tactile allodynia. Interestingly, naloxone completely abolished the analgesic effect of PSEM[89s] injection, showing that the analgesic effect of DH stimulation requires the activation of μ-opioid receptors. No effect of PSEM[89s] or naloxone was detected in sham rats (**Fig. 5F**).

Next, we aimed to identify the brain network mediating the effect of hippocampal activation on the neuropathic pain phenotype. We paired chemogenetic activation of the DH with resting-state fMRI in awake rats, chemo-fMRI (**Fig. 6A**). Spared nerve injury rats expressing PSAM in the DH received an i.p. injection of either PSEM[89s] or saline; they underwent Von Frey testing and then received 2 complete resting-state fMRI scans. Because the PSEM[89s]-induced analgesia peaked at 1 hour after injection (Supp. Fig. S1, available at http://links. lww.com/PAIN/B350), the 2 scans were completed between 60 and 90 minutes from the injection. Three hours later, the rat cohorts were swapped so that those that had received saline injections now received PSEM[89s] and vice versa, and they underwent the same protocol (injection, Von Frey test, 2 scans; **Fig. 6A**). Again, chemogenetically increasing excitability of the DH significantly blunted the SNI-induced tactile allodynia, and we then analyzed the impact of the chemogenetic activation of DH on whole brain functional network properties. We used data from both scans 1 and 2 to enhance statistical power. By examining the difference in FC of 4 seeds (PSAM injection coordinates) within the DH when the rats received either saline or PSEM[89s], we identified multiple brain

areas where connectivity with the DH was either increased or decreased following chemogenetically increasing excitability of the DH (**Figs. 6B and C**). Overall, we observed twice as many connections increasing in strength than decreasing (**Fig. 6D**). Regarding the 4 DH nodes, increased connectivity was mainly found with cortical targets, whereas decreases mostly concerned subcortical structures (Table S2, available at http:// links.lww.com/PAIN/B350). We did not detect any obvious differences in connectivity patterns between the 4 DH nodes (shown in green).

Next, we combined the results from the behavioral and the fMRI analysis to assess whether DH-driven changes in FC could be related to tactile allodynia. We first generated maps of FC changes between PSEM[89s] and saline conditions and performed a correlation analysis to directly relate these changes with changes in tactile thresholds (a list of regions is presented in Table S3, available at http://links.lww.com/PAIN/B350); 3 of these regions survived the replication step: primary somatosensory cortex (limb region), dorsolateral thalamus, and primary somatosensory cortex (barrel region; **Fig. 7A**). **Figure 7C** shows the (negative) correlation between changes in FC and allodynic threshold for discovery and replication groups for the barrel region of the primary somatosensory cortex, where we observe a negative correlation between changes in FC and in allodynic threshold of the SNI hind paw (but not for the non-SNI paw). **Figures 7D and E** show discovery and replication scatter plots for the dorsolateral thalamus (**Fig. 7D**) and the limb region of the primary somatosensory cortex (**Fig. 7E**). In both regions, discovery and replication indicate a positive correlation between changes in FC and tactile allodynia of the SNI hind paw (but no correlation for the non-SNI paw).
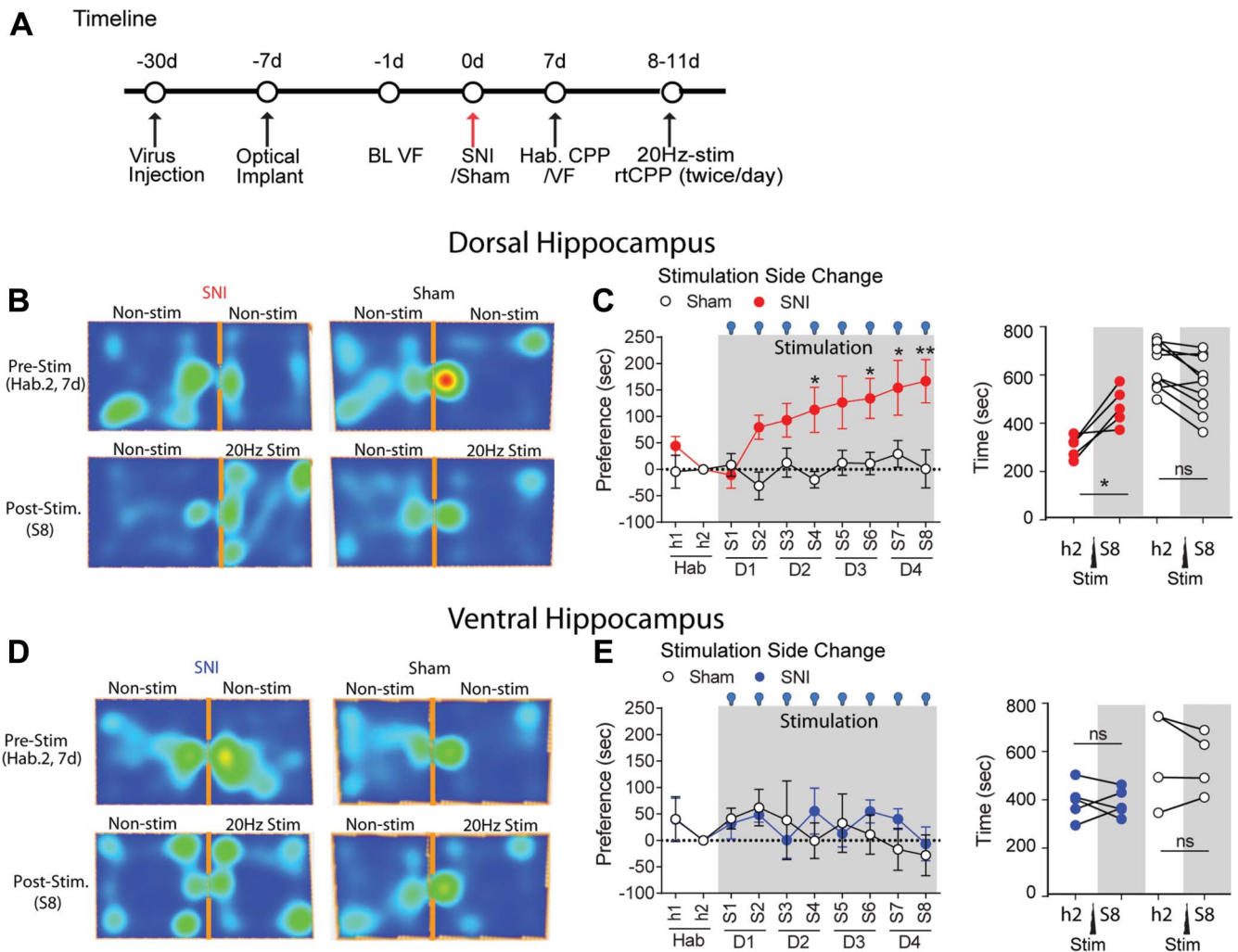
Figure 4. Activation of the dorsal, but not the ventral hippocampus is sufficient to drive preferred behavior in SNI mice. (A) Schematic representation of the behavioral paradigm for the *real-time conditioned place preference* (rtCPP) test. (B) Representative heat maps of SNI and Sham mice activity during habituation (prestimulation) and last stimulation sessions (S8) of rtCPP (20 Hz, 15 mins/session, DH optical stimulation). (C) Preference in seconds, measured by time in the stimulation-paired chamber at a given session minus time in the stimulation-paired chamber at prestimulation habituation session during rtCPP optical stimulation (20 Hz) of the dorsal hippocampus in ChR2-expressing SNI (red, n = 5) and Sham (white, n = 10) mice. (D) Representative heat maps of SNI and Sham mice activity during habituation (prestimulation) and last stimulation sessions (S8) of rtCPP (20 Hz, 15 mins/session, VH optical stimulation). (E) In contrast with dorsal hippocampus rtCPP, ventral hippocampus optical stimulation showed no preference for the stimulation-paired chamber for SNI (blue, n = 5) and Sham (n = 5) mice. Post hoc statistically significant differences are indicated as *$P < 0.05$, **$P < 0.05$, and ns $P > 0.05$ (compared with habituation, h2). For detailed statistics, see Table S1, available at http://links.lww.com/PAIN/B350. SNI, spared nerve injury.

3.4. Anterograde projections from the dorsal hippocampus and ventral hippocampus

Although projections of the DH and VH have been described,[8,26,32,36] direct examination of these projections using modern tracing methods is lacking. Therefore, in 2 mice, we traced DH (anterior or septal pole) and VH projections using the state-of-the-art anterograde labeling technique (supplementary Fig. 3, available at http://links.lww.com/PAIN/B350). The DH and VH showed nonoverlapping projections to multiple brain areas. The DH innervation of the mPFC, BLA, and VH was scarce, whereas the VH densely innervated all these areas. Projections in the septum and mamillary complex were complementary: the DH projected to the dorsal septum and the VH to the intermediate lateral and ventral septum; the DH to dorsal mammillary and the VH to ventral mammillary nuclei; the DH to the posterior dorsal ACC and the VH to the posterior ventral ACC. Both the DH and VH projected to the PAG but the VH more densely than the DH. Interestingly, although we found no projections from the DH to

VH, tracing of VH projections revealed DH terminals that were especially dense in the stratum lacunosum moleculare.

3.5. Functional connectivity of the anterior hippocampus and posterior hippocampus in humans with back pain

To explore possible human correlates of the differential involvement of the DH and VH in neuropathic pain, we tested whether the FC of the PH and AH to the cortex exhibits distinct properties in subjects with back pain. Both positive and negative FCs were studied. However, only negative FC showed regional differences. Supplementary Figure 4 demonstrates that PH-cortex negative FC was distinct between healthy controls, subjects with subacute back pain, and subjects with chronic back pain and significantly less in chronic back pain in comparison with subacute back pain. By contrast, AH-cortex negative FC did not differ between the 3 groups examined (available at http://links.lww.com/PAIN/B350).
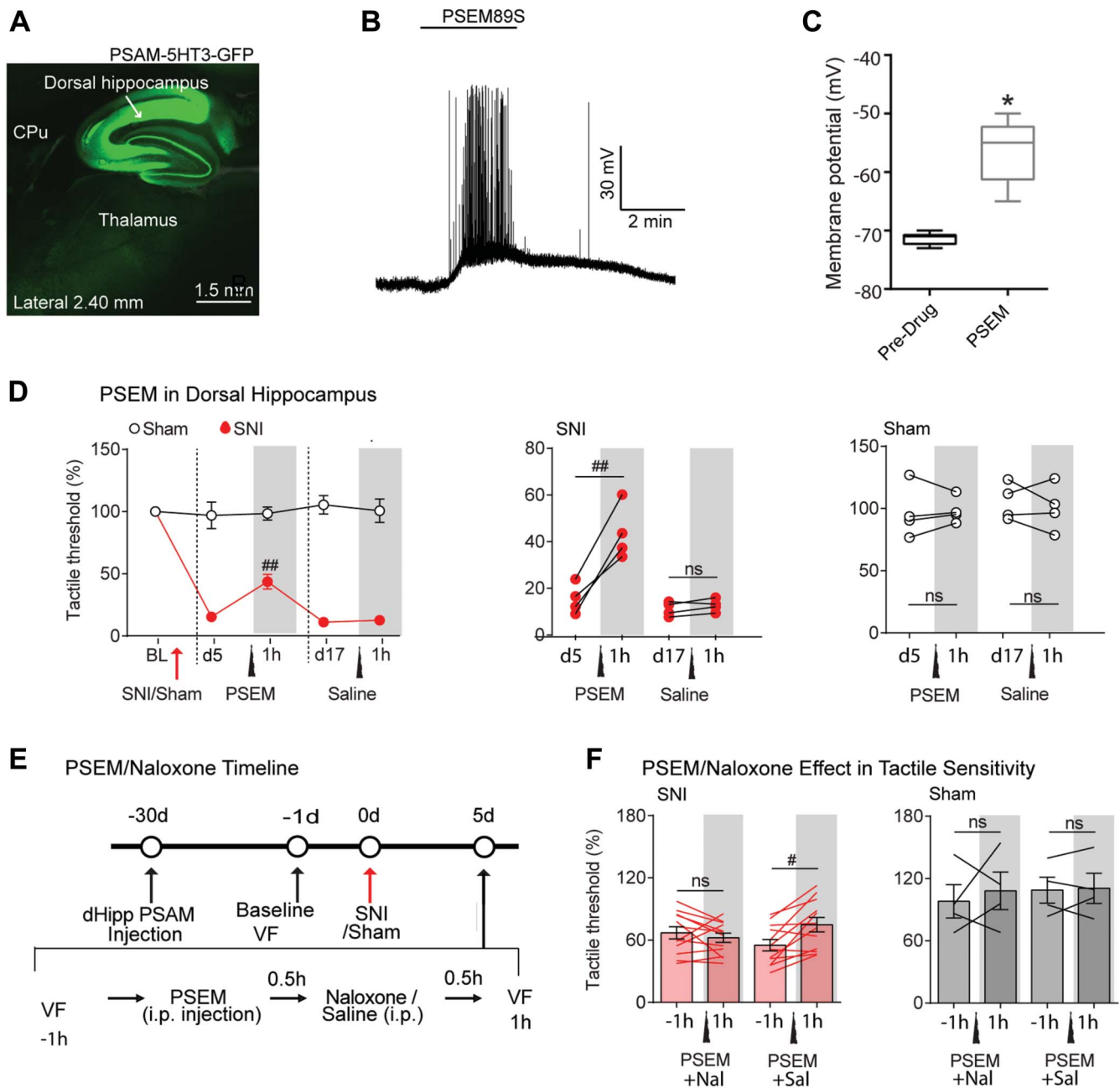
Figure 5. Chemogenetically increasing excitability of dorsal hippocampal neurons diminishes neuropathic tactile allodynia in SNI rats, abolished by naloxone. (A) In AAV—SYN-PSAM-L141F-Y115F-5HT3HC-GFP–infected rats GFP fluorescence specific for the dorsal hippocampal neurons. (B–C) Slice recording showing the rapid depolarization and spiking evoked in GFP-positive dorsal hippocampal neurons by bath application of PSEM[89s] (10 μM). (D) In PSAM-5HT3–infected SNI rats, intraperitoneal (i.p.) injection of PSEM[89s] (30 mg/kg) rapidly and reversibly blunted tactile allodynia of the SNI ipsilateral paw, on day 5 after SNI, whereas the treatment with saline did not perturb tactile sensitivity of SNI (n = 4 per group). (E) Experimental timeline: Rats were first injected with AAV9-SYN-PSAM-L141F-Y115F-5HT3HC-GFP virus into the bilateral dorsal hippocampus (~4 weeks before SNI/Sham surgeries). One day before SNI/Sham injury, tactile thresholds were assessed (baseline VF). Spared nerve injury/Sham surgeries were then performed unilaterally. Five days after surgery, tactile thresholds (−1 hour) were assessed, and afterwards, rats received PSEM[89s] injections (i.p.) followed by another i.p. injection of either naloxone or saline 30 minutes after. Tactile thresholds were assessed 1 hour after the first injection. Two days later, rats that had received PSEM[89s] and naloxone were injected with PSEM[89s] and saline, and vice versa, and tactile thresholds were assessed again. (F) PSEM[89s] injection in the virus expressed SNI rats (n = 16) showed a reduction of SNI-induced tactile allodynia. This effect was fully abolished by naloxone. By contrast, the tactile threshold of sham rats (n = 4) was unchanged by naloxone. Post hoc statistically significant differences are indicated as follows: #$P < 0.01$, ##$P < 0.05$, * < 0.05, and ns $P > 0.05$ (between before and after PSEM or saline ± naloxone or saline). For detailed statistics, see Table S1, available at http://links.lww.com/PAIN/B350. rtCPP, real-time conditioned place preference; SNI, spared nerve injury.

4. Discussion

We used a multiplicity of strategies to investigate the respective roles of the DH and VH in neuropathic pain in rats and mice. The main results of our study are (1) *activation* of the DH, but not the VH, had analgesic effects in SNI (and SNL), but not sham-operated,

mice (and rats) regarding tactile sensitivity and motivated behavior; (2) pharmacological *inhibition* of the DH had proalgesic effects in sham-operated, but not SNI, mice; (3) the analgesic effect of DH stimulation in SNI mice was NMDA dependent and required activation of μ-opioid receptors; and (4) chemogenetically increasing excitability of DH neurons was sufficient to induce
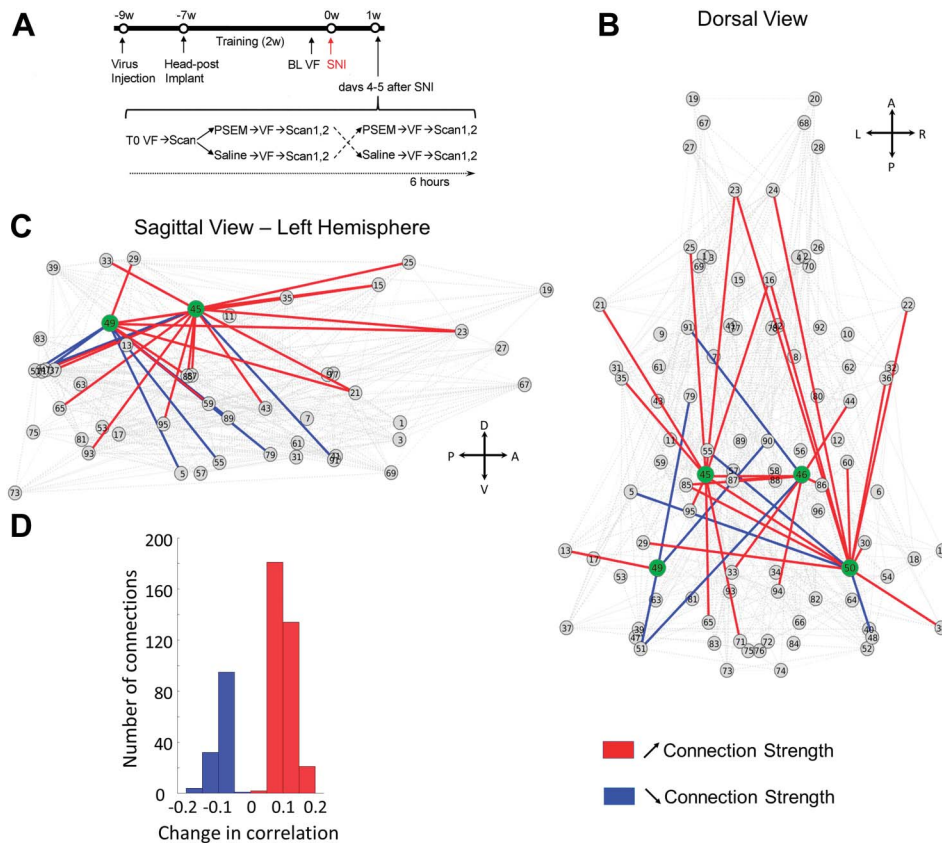
Figure 6. Awake chemo-fMRI functional network reorganization with increasing excitability of the dorsal hippocampus (DH) in rats: Subdividing the brain into 96 clusters identifies whole-brain and dorsal hippocampus connectivity changes with increased DH excitability. (A) Experimental timeline: Rats (n = 7) were first injected with AAV9-SYN-PSAM-L141F-Y115F-5HT3HC-GFP virus into the bilateral dorsal hippocampus (~9 weeks before SNI surgery). Two weeks later, they received head-posts (~7 weeks) and then underwent a 2-week training period to enable awake resting-state fMRI; 1 to 2 days before SNI injury, baseline tactile thresholds were assessed for left and right hind paws (BL VF). Spared nerve injury surgery was then performed unilaterally. Four or 5 days after surgery, tactile thresholds (T0) were assessed, and the rats scanned for resting-state fMRI (rsfMRI); immediately afterwards, rats received either saline or PSEM[89s] injections (i.p.), retested for tactile thresholds, and again underwent awake rsfMRI (2 consecutive scans). Two hours later, rats that had received PSEM[89s] were injected with saline, and vice versa, and tactile thresholds and rsfMRI were assessed one more time. (B–C), Dorsal and lateral views of change in network connectivity with increased DH excitability, comparing PSEM[89s] with the saline injection conditions. Change in connectivity across all nodes is shown in gray; increased and decreased connectivity for the 4 DH seeds (green) are shown in red and blue, respectively. (D) Histogram of the significant changes in the average correlation coefficient for PSEM[89s] in contrast to saline: Contrasts were performed combining scan 1 and 2 data, using permutation testing, $P < 0.05$ (see Table S2 for statistical details, available at http://links.lww.com/PAIN/B350). A, anterior; D, dorsal; L, left; P, posterior; R, right; SNI, spared nerve injury; V, ventral.

analgesia in SNI rats. Awake resting-state chemo-fMRI identified underlying functional network changes, and DH functional connections to the thalamus and somatosensory cortex correlated with observed analgesia. Together, these results show a causal relationship between DH, but not VH, neural activity in neuropathic pain and imply that the DH local circuitry and FC are deactivated in neuropathic pain. In addition, we show evidence for the DH and VH exhibiting distinct anatomical projections in the mouse and in humans negative FC showing distinct properties in the AH and PH between healthy, subacute, and chronic back pain subjects.

4.1. Neuropathic pain along the long axis of the hippocampus—rodent studies

Functional segregation along the long axis of the hippocampus remains an evolving topic.[54] There may be important differences in this organization between primates and rodents, and it remains unclear the extent to which functional differences constitute a gradient or comprise a constellation of discrete modules or some combination of both.[56,70] Studies of hippocampal abnormalities and their contribution to rodent models of chronic pain are rapidly increasing. Yet, majority concentrate on abnormalities in

cognitive, memory, anxiety, and depression-like behaviors (see Refs 10,14,22,28,38,39,69,72,77,79,81,83). The current results are the first to suggest a strict dichotomy between the DH and VH regarding neuropathic pain. Yet, within the DH, an exact location, specific neuronal populations, and underlying intrinsic circuitry controlling neuropathic pain remain unknown.

The DH plays a well-established role in episodic memories.[25,57,71] We recently demonstrated that the valence (positive and negative value) of memory traces within the DH is mediated by glutamatergic projections from the ventral tegmental area.[30] Thus, this pathway may be a route for reorganizing DH circuits with neuropathic pain, specifically regarding the motivational/emotional value control, which we could demonstrate in opto-rtCPP experiments. However, activation of the ventral tegmental area is not sufficient to induce reward-related behavioral responses,[30] suggesting that other additional inputs must also be involved. Regarding DH outputs and neuropathic pain, the chemo-fMRI evidence showed that increasing DH excitability leads to increased positive and negative FC to many brain targets, and FC to the thalamus and somatosensory cortex reflected changes in tactile allodynia, likely mediated through multisynaptic pathways because there are no known direct DH projections to these regions.
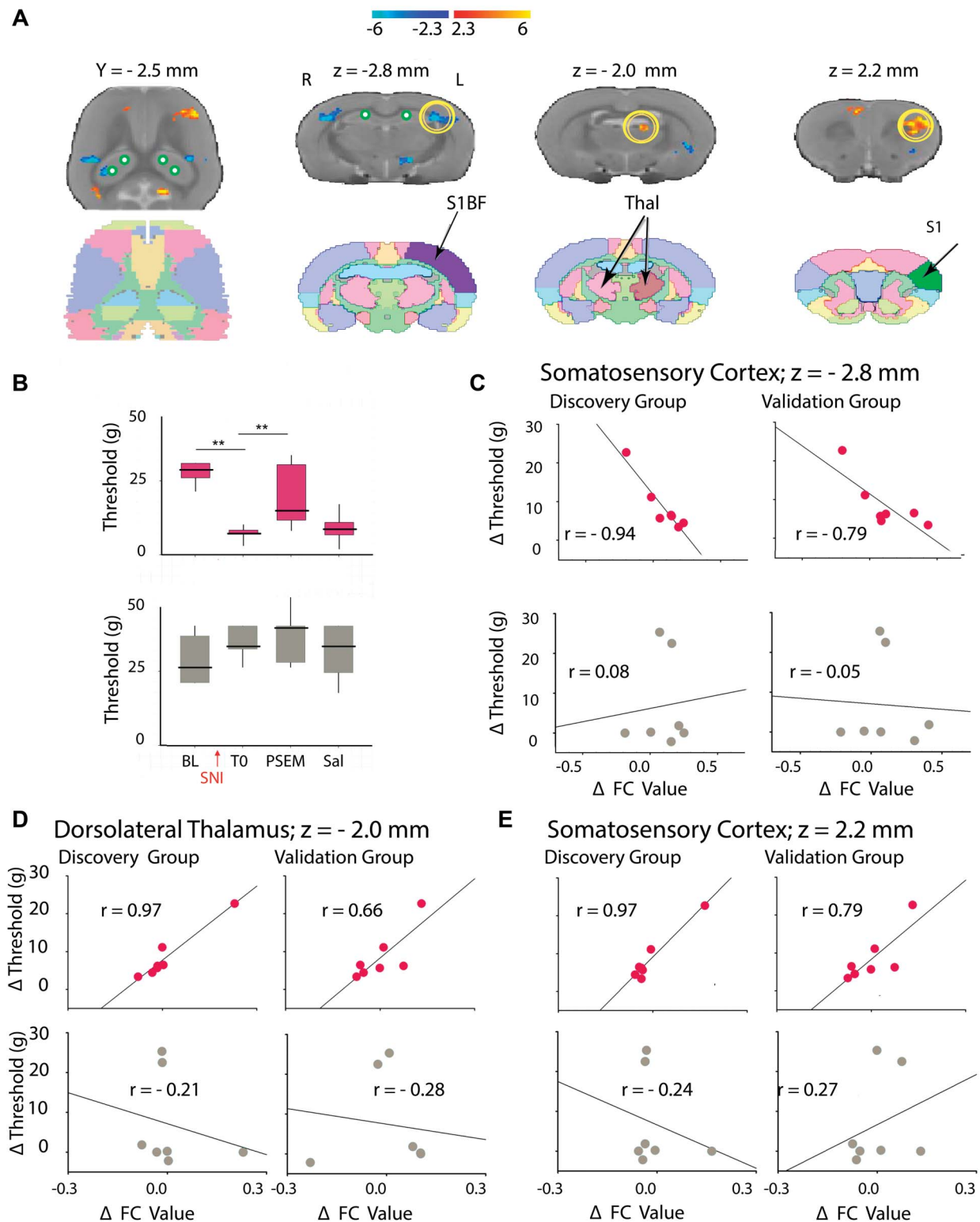
Figure 7. Awake chemo-fMRI identifies dorsal hippocampal–driven functional networks that reflect change in tactile allodynia as a function of increased dorsal hippocampal excitability in rats. (A) The map delineates brain regions where functional connectivity changes (ΔFC; between PSEM and saline conditions) were correlated with change in tactile allodynia (ΔThreshold; between PSEM and saline conditions), for stimulating the SNI hind paw (using only scan 1 data) (cluster corrected for multiple comparisons. Table S3, available at http://links.lww.com/PAIN/B350, summarizes identified regions and associated statistics). Standard atlas slices are also illustrated. (B) Group median (quartiles and minimum/maximum) tactile thresholds are shown, for the SNI hind paw (red) and healthy hind paw (gray). Tactile thresholds for the SNI hind paw diminished at 1 hour after PSEM[89s], but not after saline. Post hoc comparisons **P < 0.01 (between baseline and post-SNI, T0; also between T0 SNI and SNI + PSEM). (C) Average scatter plots across all 4 seeds for the primary somatosensory cortex (barrel field) between ΔFC and ΔThreshold are shown for discovery and replication groups for the SNI (red) and healthy hind paw (gray). We observe the SNI hind paw ΔThreshold is negatively correlated with the average ΔFC, but not for the non-SNI hind paw. Thus, we consider this brain regional FC a reliable outcome, indicating that high FC values in the region are related with high neuropathic pain (yellow circle at z = −2.8 mm in (A)). (D and E) Two additional brain regions identified in the discovery data could be replicated (yellow circles at z = −2.0 mm and z = 2.0 mm in (A)). In both regions, dorsolateral thalamus (D) and primary somatosensory cortex (limb region) (E), discovery and replication results show a positive relationship between ΔFC and ΔThreshold for the SNI hind paw, but not for the non-SNI hind paw. Thus, in these 2 regions, high FC values (in PSEM[89s]) are associated with decreased neuropathic pain. Only across-seeds group averages are displayed. SNI, spared nerve injury.

Although activation of the VH did not modulate neuropathic pain, other evidence suggests that it undergoes reorganization and may contribute to anxiety/depression-type behaviors commonly associated with neuropathic pain. The VH exhibits neuroimmune activation after peripheral nerve injury and enhanced anxiety in susceptible animals.[28] Mice with persistent neuropathic pain show reduced active neural stem cells in the VH dentate gyrus and heightened anxiety, and fluoxetine increases the proliferation of active neural stem cells and alleviates anxiety without effecting tactile allodynia.[83] Complimenting these observations, we have shown a dissociation between neuropathic pain behavior and depression-like behaviors in transgenic mice, coupled with reduced neurogenesis and diminished learning abilities.[3] We have also shown that the synaptic strength of VH projections to the nucleus accumbens medial shell (D2-receptor expressing spiny projection neurons) is enhanced after SNI, and increasing excitability of these neurons exacerbates neuropathic pain.[60,61] However, because activation of the VH did not modulate neuropathic pain, the VH to the accumbens synapses by themselves is not sufficient to modify neuropathic behavior. Altogether, it seems that both the DH and VH undergo reorganization with neuropathic pain; the DH circuitry undergoes deactivation and exhibits ability to control neuropathic pain, whereas the VH shows increased connectivity contributing to anxiety/depression-like behaviors.

4.2. Chronic pain along the long axis of the hippocampus—human studies

In parallel and complimenting the rodent studies, human neuroimaging studies show hippocampal structural and functional abnormalities in various types of chronic pain.[4,9,24,31,40,66,75] Our studies indicate that hippocampal volume[73,74] and positive FC from the AH to the cortex[48,59] are both prognostic biomarkers for transition to chronic back pain. Moreover, a suborportion of AH undergoes outward shape deformation in females transitioning to chronic back pain.[58] Importantly, a specific AH-cortex positive FC changes over time in proportion to changes in back pain[48] (which parallels increased VH-accumbens connectivity in SNI); a result recently replicated using a meta-analysis approach.[4] Thus, the bulk of prior evidence points to AH reorganization with chronic pain. Therefore, here, we re-examined our human data specifically to contrast FC between the AH and PH. The results indicate distinct reorganization for negative FC, demonstrating opposite patterns of reorganization in the AH and PH (in similarity to rodents with SNI). Earlier results indicate in chronic back pain that a specific PH regional shape is tightly related to the mismatch between experienced pain and its memory.[7] Thus, it is likely that the differences we see of PH-cortex negative FC may reflect pain memory distortions in back pain.

4.3. What cellular mechanisms mediate the DH effect?

Our results are consistent with older observations. Rodent studies show decreased excitability of dorsal hippocampus CA1 pyramidal neurons and increased GABAergic activity in the formalin pain model,[34] and electrical stimulation of the DH leads to antinociceptive behaviors.[55] Abnormal hippocampal glutamatergic activity[78] and decreased hippocampal long-term potentiation are observed in neuropathic rats.[37] After chronic constriction injury, hippocampal CA1 glutamate concentration is decreased, whereas GABA concentration is increased and correlated with pain thresholds.[63] Also, DH inhibition of the GABAergic system by bicuculline increases antinociception,

whereas muscimol promotes pronociception.[27] Thus, microinjection of glutamate in the dorsal hippocampus may reverse neuropathic pain by rebalancing local excitatory/inhibitory neurotransmitters.

Spared nerve injury animals are unable to extinguish contextual fear, which is associated with decreased hippocampal neurogenesis and impaired plasticity.[49] This may suggest that the same DH dysfunctions that drive neuropathic pain also mediate the failure to extinguish fear. Such mechanisms include impaired synaptic plasticity,[49] likely mediated by NMDA channels.[44] In keeping with the hypothesis that synaptic plasticity, rather than simple cellular excitation, is critical for this effect; our present data show that NMDA blockade prevents the analgesia observed with DH activation. In addition, the persistence of the glutamate analgesia (consistent with the reduction of glutamate and glutamate transporter levels in the hippocampus in SNI[80]) further supports a critical role of long-term synaptic regulation. The potential site of this plasticity and its polarity remain unknown, but previous work shows LTP impairment in the DH.[62] Interestingly, we found that analgesic effect caused in SNI rats by activation of the DH was abolished by naloxone. Although it is likely that the μ-opioid receptor sensitivity of the DH-dependent analgesia is the result of activation of descending modulatory pathways, hippocampal plasticity itself is modulated by endogenous opioids,[45] and the 2 modulations are not mutually exclusive.

4.4. Advantages and limitations

The main strength of our study resides in the consistency of the results obtained using multiplicity of approaches, models, and species. Each of the 3 brain modulation techniques used has advantages and disadvantages; the major advantage of the pharmacological modulation is that it identifies molecular targets (the ligand receptors) that mediate the observed effects. A potential problem, however, is that different cell types (including glia) are simultaneously affected; in addition, it is unclear how much tissue was affected. Optogenetic stimulation is typically used to activate specific axon terminals. Here, we used it to excite local cell bodies; it may be argued that our optogenetic results share some of the same concerns as in the pharmacological approach. A critical advantage of our experimental design was *wireless* optogenetic stimulation to assess *real-time place* preference. This approach allows assessing rodents' behavior in more physiological conditions than the traditional fiber-implanted systems[43] and to determine the behavioral effects in real time. The chemo-fMRI approach is, to the best of our knowledge, the only one that allows the identification of changes in FC caused by selectively increasing excitability of a specific brain area. Thus, although each of our approaches has limitations, their combined use yielding convergent evidence imparts high confidence of main results.

5. Conclusions

Over a decade ago, we launched human and rodent studies to link hippocampal processes with chronic pain based on the theoretical formulation that chronic pain may be envisioned as a state of extinction-resistant emotional learning.[2] Current results are consistent with this concept but only indirectly. Our primary conclusion is that the DH is deactivated with neuropathic pain, which unmasks DH control of both tactile allodynia and motivational/affective properties of neuropathic pain. Thus, the DH/PH should be considered a critical hub for novel treatment options for chronic pain.

Appendix A. Supplemental digital content

Supplemental digital content associated with this article can be found online at http://links.lww.com/PAIN/B350.

References

[1] Adhikari A. Distributed circuits underlying anxiety. Front Behav Neurosci 2014;8:112.
[2] Apkarian AV. Pain perception in relation to emotional learning. CurrOpinNeurobiol 2008;18:464–8.
[3] Apkarian AV, Mutso AA, Centeno MV, Kan L, Wu M, Levinstein M, Banisadr G, Gobeske KT, Miller RJ, Radulovic J, Hen R, Kessler JA. Role of adult hippocampal neurogenesis in persistent pain. PAIN 2016;157:418–28.
[4] Ayoub LJ, Barnett A, Leboucher A, Golosky M, McAndrews MP, Seminowicz DA, Moayedi M. The medial temporal lobe in nociception: a meta-analytic and functional connectivity study. PAIN 2019;160:1245–60.
[5] Baliki MN, Chang PC, Baria AT, Centeno MV, Apkarian AV. Resting-sate functional reorganization of the rat limbic system following neuropathic injury. Sci Rep 2014;4:6186.
[6] Bennett GJ, Xie YK. A peripheral mononeuropathy in rat that produces disorders of pain sensation like those seen in man. PAIN 1988;33:87–107.
[7] Berger SE, Vachon-Presseau E, Abdullah TB, Baria AT, Schnitzer TJ, Apkarian AV. Hippocampal morphology mediates biased memories of chronic pain. Neuroimage 2018;166:86–98.
[8] Bienkowski MS, Bowman I, Song MY, Gou L, Ard T, Cotter K, Zhu M, Benavidez NL, Yamashita S, Abu-Jaber J, Azam S, Lo D, Foster NN, Hintiryan H, Dong HW. Integration of gene expression and brain-wide connectivity reveals the multiscale organization of mouse hippocampal networks. Nat Neurosci 2018;21:1628–43.
[9] Bishop JH, Shpaner M, Kubicki A, Clements S, Watts R, Naylor MR. Structural network differences in chronic musculoskeletal pain: beyond fractional anisotropy. Neuroimage 2018;182:441–55.
[10] Cardenas A, Caniglia J, Keljalic D, Dimitrov E. Sex differences in the development of anxiodepressive-like behavior of mice subjected to sciatic nerve cuffing. PAIN 2020;161:1861–71.
[11] Cardoso-Cruz H, Dourado M, Monteiro C, Galhardo V. Blockade of dopamine D2 receptors disrupts intrahippocampal connectivity and enhances pain-related working memory deficits in neuropathic pain rats. Eur J Pain 2018;22:1002–15.
[12] Cardoso-Cruz H, Dourado M, Monteiro C, Matos MR, Galhardo V. Activation of dopaminergic D2/D3 receptors modulates dorsoventral connectivity in the hippocampus and reverses the impairment of working memory after nerve injury. J Neurosci 2014;34:5861–73.
[13] Cardoso-Cruz H, Lima D, Galhardo V. Instability of spatial encoding by CA1 hippocampal place cells after peripheral nerve injury. Eur J Neurosci 2011;33:2255–64.
[14] Cardoso-Cruz H, Paiva P, Monteiro C, Galhardo V. Bidirectional optogenetic modulation of prefrontal-hippocampal connectivity in pain-related working memory deficits. Sci Rep 2019;9:10980.
[15] Chang PC, Centeno MV, Procissi D, Baria A, Apkarian AV. Brain activity for tactile allodynia: a longitudinal awake rat functional magnetic resonance imaging study tracking emergence of neuropathic pain. PAIN 2017;158:488–97.
[16] Chang PC, Pollema-Mays SL, Centeno MV, Procissi D, Contini M, Baria AT, Martina M, Apkarian AV. Role of nucleus accumbens in neuropathic pain: linked multi-scale evidence in the rat transitioning to neuropathic pain. PAIN 2014;155:1128–39.
[17] Chang PC, Procissi D, Bao Q, Centeno MV, Baria A, Apkarian AV. Novel method for functional brain imaging in awake minimally restrained rats. J Neurophysiol 2016;116:61–80.
[18] Chaplan SR, Bach FW, Pogrel JW, Chung JM, Yaksh TL. Quantitative assessment of tactile allodynia in the rat paw. J Neurosci Methods 1994;53:55–63.
[19] Ciocchi S, Passecker J, Malagon-Vina H, Mikus N, Klausberger T. Brain computation. Selective information routing by ventral hippocampal CA1 projection neurons. Science 2015;348:560–3.
[20] Decosterd I, Woolf CJ. Spared nerve injury: an animal model of persistent peripheral neuropathic pain. PAIN 2000;87:149–58.
[21] del Rey A, Yau HJ, Randolf A, Centeno MV, Wildmann J, Martina M, Besedovsky HO, Apkarian AV. Chronic neuropathic pain-like behavior correlates with IL-1beta expression and disrupts cytokine interactions in the hippocampus. PAIN 2011;152:2827–35.
[22] Egorova E, Starinets A, Tyrtyshnaia A, Ponomarenko A, Manzhulo I. Hippocampal neurogenesis in conditions of chronic stress induced by sciatic nerve injury in the rat. Cells Tissues Organs 2019;207:58–68.
[23] Eichenbaum H, Cohen NJ. Can we reconcile the declarative memory and spatial navigation views on hippocampal function? Neuron 2014;83:764–70.
[24] Ezzati A, Zammit AR, Lipton ML, Lipton RB. The relationship between hippocampal volume, chronic pain, and depressive symptoms in older adults. Psychiatry Res Neuroimaging 2019;289:10–12.
[25] Fanselow MS. Contextual fear, gestalt memories, and the hippocampus. Behav Brain Res 2000;110:73–81.
[26] Fanselow MS, Dong HW. Are the dorsal and ventral hippocampus functionally distinct structures? Neuron 2010;65:7–19.
[27] Favaroni Mendes LA, Menescal-de-Oliveira L. Role of cholinergic, opioidergic and GABAergic neurotransmission of the dorsal hippocampus in the modulation of nociception in guinea pigs. Life Sci 2008;83:644–50.
[28] Fiore NT, Austin PJ. Peripheral nerve injury triggers neuroinflammation in the medial prefrontal cortex and ventral Hippocampus in a subgroup of rats with coincident affective behavioural changes. Neuroscience 2019;416:147–67.
[29] Gurtskaia G, Tsiklauri N, Nozadze I, Nebieridze M, Tsagareli MG. Antinociceptive tolerance to NSAIDs microinjected into dorsal hippocampus. BMC Pharmacol Toxicol 2014;15:10.
[30] Han Y, Zhang Y, Kim H, Grayson VS, Jovasevic V, Ren W, Centeno MV, Guedea AL, Meyer MAA, Wu Y, Gutruf P, Surmeier DJ, Gao C, Martina M, Apkarian AV, Rogers JA, Radulovic J. Excitatory VTA to DH projections provide a valence signal to memory circuits. Nat Commun 2020;11:1466.
[31] Hu C, Yang H, Zhao Y, Chen X, Dong Y, Li L, Dong Y, Cui J, Zhu T, Zheng P, Lin CS, Dai J. The role of inflammatory cytokines and ERK1/2 signaling in chronic prostatitis/chronic pelvic pain syndrome with related mental health disorders. Sci Rep 2016;6:28608.

[32] Jay TM, Witter MP. Distribution of hippocampal CA1 and subicular efferents in the prefrontal cortex of the rat studied by means of anterograde transport of Phaseolus vulgaris-leucoagglutinin. J Comp Neurol 1991;313:574–86.

[33] Jimenez JC, Su K, Goldberg AR, Luna VM, Biane JS, Ordek G, Zhou P, Ong SK, Wright MA, Zweifel L, Paninski L, Hen R, Kheirbek MA. Anxiety cells in a hippocampal-hypothalamic circuit. Neuron 2018;97: 670–83.e676.

[34] Khanna S. Dorsal hippocampus field CA1 pyramidal cell responses to a persistent versus an acute nociceptive stimulus and their septal modulation. Neuroscience 1997;77:713–21.

[35] Kim SH, Chung JM. An experimental model for peripheral neuropathy produced by segmental spinal nerve ligation in the rat. PAIN 1992;50: 355–63.

[36] Kishi T, Tsumori T, Yokota S, Yasui Y. Topographical projection from the hippocampal formation to the amygdala: a combined anterograde and retrograde tracing study in the rat. J Comp Neurol 2006;496:349–68.

[37] Kodama D, Ono H, Tanabe M. Altered hippocampal long-term potentiation after peripheral nerve injury in mice. Eur J Pharmacol 2007; 574:127–32.

[38] Li L, Zou Y, Liu B, Yang R, Yang J, Sun M, Li Z, Xu X, Li G, Liu S, Greffrath W, Treede RD, Li G, Liang S. Contribution of the P2X4 receptor in rat Hippocampus to the comorbidity of chronic pain and depression. ACS Chem Neurosci 2020;11:4387–97.

[39] Li Q, Liu S, Zhu X, Mi W, Maoying Q, Wang J, Yu J, Wang Y. Hippocampal PKR/NLRP1 inflammasome pathway is required for the depression-like behaviors in rats with neuropathic pain. Neuroscience 2019;412:16–28.

[40] Lisicki M, D'Ostilio K, Coppola G, Parisi V, de Noordhout AM, Magis D, Schoenen J, Scholtes F, Versijpt J. Age related metabolic modifications in the migraine brain. Cephalalgia 2019;39:978–87.

[41] Liu X, Ramirez S, Tonegawa S. Inception of a false memory by optogenetic manipulation of a hippocampal memory engram. Philos Trans R Soc Lond Ser B Biol Sci 2014;369:20130142.

[42] Liu Y, Zhou LJ, Wang J, Li D, Ren WJ, Peng J, Wei X, Xu T, Xin WJ, Pang RP, Li YY, Qin ZH, Murugan M, Mattson MP, Wu LJ, Liu XG. TNF-alpha differentially regulates synaptic plasticity in the Hippocampus and spinal cord by microglia-dependent mechanisms after peripheral nerve injury. J Neurosci 2017;37:871–81.

[43] Lu L, Gutruf P, Xia L, Bhatti DL, Wang X, Vazquez-Guardado A, Ning X, Shen X, Sang T, Ma R, Pakeltis G, Sobczak G, Zhang H, Seo DO, Xue M, Yin L, Chanda D, Sheng X, Bruchas MR, Rogers JA. Wireless optoelectronic photometers for monitoring neuronal dynamics in the deep brain. Proc Natl Acad Sci United States America 2018;115: E1374–83.

[44] Malenka RC, Nicoll RA. NMDA-receptor-dependent synaptic plasticity: multiple forms and mechanisms. Trends Neurosciences 1993;16:521–7.

[45] Morris BJ, Johnston HM. A role for hippocampal opioids in long-term functional plasticity. Trends Neurosciences 1995;18:350–5.

[46] Moser EI, Moser MB, McNaughton BL. Spatial representation in the hippocampal formation: a history. Nat Neurosci 2017;20:1448–64.

[47] Moser MB, Moser EI. Distributed encoding and retrieval of spatial memory in the hippocampus. J Neurosci 1998;18:7535–42.

[48] Mutso AA, Petre B, Huang L, Baliki MN, Torbey S, Herrmann K, Schnitzer TJ, Apkarian AV. Reorganization of hippocampal functional connectivity with transition to chronic back pain. J Neurophysiol 2014;111:1065–76.

[49] Mutso AA, Radzicki D, Baliki MN, Huang L, Banisadr G, Centeno MV, Radulovic J, Martina M, Miller RJ, Apkarian AV. Abnormalities in hippocampal functioning with persistent pain. J Neurosci 2012;32: 5747–56.

[50] O'Leary OF, Cryan JF. A ventral view on antidepressant action: roles for adult hippocampal neurogenesis along the dorsoventral axis. Trends Pharmacol Sci 2014;35:675–87.

[51] Papatheodoropoulos C. Electrophysiological evidence for long-axis intrinsic diversification of the hippocampus. Front Biosci 2018;23: 109–45.

[52] Paxinos GWC. The rat brain in stereotaxic coordinates. San Diego, CA: Academic Press, 1997.

[53] Petroski RE, Pomeroy JE, Das R, Bowman H, Yang W, Chen AP, Foster AC. Indiplon is a high-affinity positive allosteric modulator with selectivity for alpha1 subunit-containing GABAA receptors. J Pharmacol Exp Ther 2006;317:369–77.

[54] Poppenk J, Evensmoen HR, Moscovitch M, Nadel L. Long-axis specialization of the human hippocampus. Trends Cogn Sci 2013;17: 230–40.

[55] Prado WA, Roberts MH. An assessment of the antinociceptive and aversive effects of stimulating identified sites in the rat brain. Brain Res 1985;340:219–28.

[56] Qin S, Duan X, Supekar K, Chen H, Chen T, Menon V. Large-scale intrinsic functional network organization along the long axis of the human medial temporal lobe. Brain Struct Funct 2016;221:3237–58.

[57] Quinn JJ, Loya F, Ma QD, Fanselow MS. Dorsal hippocampus NMDA receptors differentially mediate trace and contextual fear conditioning. Hippocampus 2005;15:665–74.

[58] Reckziegel D, Abdullah T, Wu B, Wu B, Huang L, Schnitzer TJ, Apkarian AV. Hippocampus shape deformation: a potential diagnostic biomarker for chronic back pain in women. PAIN 2021;162:1457–67.

[59] Reckziegel DT P, Apkarian AV. Gender dependent pharmacotherapy for blocking transition to chronic back pain: a proof of concept randomized trial. medrxiv 2019. doi: https://doi.org/10.1101/19006627.

[60] Ren W, Centeno MV, Berger S, Wu Y, Na X, Liu X, Kondapalli J, Apkarian AV, Martina M, Surmeier DJ. The indirect pathway of the nucleus accumbens shell amplifies neuropathic pain. Nat Neurosci 2016;19: 220–2.

[61] Ren W, Centeno MV, Wei X, Wickersham I, Martina M, Apkarian AV, Surmeier DJ. Adaptive alterations in the mesoaccumbal network following peripheral nerve injury. PAIN 2020.

[62] Ren WJ, Liu Y, Zhou LJ, Li W, Zhong Y, Pang RP, Xin WJ, Wei XH, Wang J, Zhu HQ, Wu CY, Qin ZH, Liu G, Liu XG. Peripheral nerve injury leads to working memory deficits and dysfunction of the Hippocampus by upregulation of TNF-alpha in rodents. Neuropsychopharmacology 2011;36:979–92.

[63] Saffarpour S, Shaabani M, Naghdi N, Farahmandfar M, Janzadeh A, Nasirinezhad F. In vivo evaluation of the hippocampal glutamate, GABA and the BDNF levels associated with spatial memory performance in a rodent model of neuropathic pain. Physiol Behav 2017;175:97–103.

[64] Sapolsky RM, Krey LC, McEwen BS. Prolonged glucocorticoid exposure reduces hippocampal neuron number: implications for aging. J Neurosci 1985;5:1222–7.

[65] Satpute AB, Mumford JA, Naliboff BD, Poldrack RA. Human anterior and posterior hippocampus respond distinctly to state and trait anxiety. Emotion 2012;12:58–68.

[66] Schreiber KL, Loggia ML, Kim J, Cahalan CM, Napadow V, Edwards RR. Painful after-sensations in fibromyalgia are linked to catastrophizing and differences in brain response in the medial temporal lobe. J Pain 2017;18: 855–67.

[67] Schwarz AJ, Danckaert A, Reese T, Gozzi A, Paxinos G, Watson C, Merlo-Pich EV, Bifone A. A stereotaxic MRI template set for the rat brain with tissue class distribution maps and co-registered anatomical atlas: application to pharmacological MRI. Neuroimage 2006;32:538–50.

[68] Shin G, Gomez AM, Al-Hasani R, Jeong YR, Kim J, Xie Z, Banks A, Lee SM, Han SY, Yoo CJ, Lee JL, Lee SH, Kurniawan J, Tureb J, Guo Z, Yoon J, Park SI, Bang SY, Nam Y, Walicki MC, Samineni VK, Mickle AD, Lee K, Heo SY, McCall JG, Pan T, Wang L, Feng X, Kim TI, Kim JK, Li Y, Huang Y, RWt Gereau, Ha JS, Bruchas MR, Rogers JA. Flexible near-field wireless optoelectronics as subdermal implants for broad applications in optogenetics. Neuron 2017;93:509–21.e503.

[69] Slivicki RA, Mali SS, Hohmann AG. Voluntary exercise reduces both chemotherapy-induced neuropathic nociception and deficits in hippocampal cellular proliferation in a mouse model of paclitaxel-induced peripheral neuropathy. Neurobiol Pain 2019;6:100035.

[70] Strange BA, Witter MP, Lein ES, Moser EI. Functional organization of the hippocampal longitudinal axis. Nat Rev Neurosci 2014;15:655–69.

[71] Tulving E. Multiple memory systems and consciousness. Hum Neurobiol 1987;6:67–80.

[72] Tyrtyshnaia AA, Manzhulo IV, Konovalova SP, Zagliadkina AA. Neuropathic pain causes a decrease in the dendritic tree complexity of hippocampal CA3 pyramidal neurons. Cells Tissues Organs 2019;208: 89–100.

[73] Vachon-Presseau E, Centeno MV, Ren W, Berger SE, Tetreault P, Ghantous M, Baria A, Farmer M, Baliki MN, Schnitzer TJ, Apkarian AV. The emotional brain as a predictor and amplifier of chronic pain. J Dent Res 2016;95:605–12.

[74] Vachon-Presseau E, Tetreault P, Petre B, Huang L, Berger SE, Torbey S, Baria AT, Mansour AR, Hashmi JA, Griffith JW, Comasco E, Schnitzer TJ, Baliki MN, Apkarian AV. Corticolimbic anatomical characteristics predetermine risk for chronic pain. Brain 2016;139:1958–70.

[75] Vaculik MF, Noorani A, Hung PS, Hodaie M. Selective hippocampal subfield volume reductions in classic trigeminal neuralgia. Neuroimage Clin 2019;23:101911.

[76] Vogel JW, La Joie R, Grothe MJ, Diaz-Papkovich A, Doyle A, Vachon-Presseau E, Lepage C, Vos de Wael R, Thomas RA, Iturria-Medina Y, Bernhardt B, Rabinovici GD, Evans AC. A molecular gradient along the longitudinal axis of the human hippocampus informs large-scale behavioral systems. Nat Commun 2020;11:960.

[77] Wang XM, Zhang GF, Jia M, Xie ZM, Yang JJ, Shen JC, Zhou ZQ. Environmental enrichment improves pain sensitivity, depression-like phenotype, and memory deficit in mice with neuropathic pain: role of NPAS4. Psychopharmacology 2019;236:1999–2014.

[78] Wang XQ, Zhong XL, Li ZB, Wang HT, Zhang J, Li F, Zhang JY, Dai RP, Xin-Fu Z, Li CQ, Li ZY, Bi FF. Differential roles of hippocampal glutamatergic receptors in neuropathic anxiety-like behavior after partial sciatic nerve ligation in rats. BMC Neurosci 2015;16:14.

[79] Xiong B, Zhang W, Zhang L, Huang X, Zhou W, Zou Q, Manyande A, Wang J, Tian Y, Tian X. Hippocampal glutamatergic synapses impairment mediated novel-object recognition dysfunction in rats with neuropathic pain. PAIN 2020;161:1824–36.

[80] Xiong B, Zhang W, Zhang L, Huang X, Zhou W, Zou Q, Manyande A, Wang J, Tian Y, Tian X. Hippocampal glutamatergic synapses impairment mediated novel-object recognition dysfunction of neuropathic pain in rats. PAIN 2020;161:1824–36.

[81] Zhang GF, Zhou ZQ, Guo J, Gu HW, Su MZ, Yu BC, Zhou F, Han BY, Jia M, Ji MH, Tao YX, Zhao CJ, Yang JJ. Histone deacetylase 3 in hippocampus contributes to memory impairment after chronic constriction injury of sciatic nerve in mice. PAIN 2021;162:382–95.

[82] Zhang M, Liu J, Zhou MM, Wu H, Hou Y, Li YF, Yin Y, Zheng L, Cai J, Liao FF, Liu FY, Yi M, Wan Y. Anxiolytic effects of hippocampal neurosteroids in normal and neuropathic rats with spared nerve injury. J Neurochem 2017;141:137–50.

[83] Zhao Y, Zhang L, Wang M, Yu J, Yang J, Liu A, Yao H, Liu X, Shen Y, Guo B, Wang Y, Wu S. Anxiety specific response and contribution of active hippocampal neural stem cells to chronic pain through Wnt/beta-catenin signaling in mice. Front Mol Neurosci 2018;11:296.